Acta metall. mater. Vol. 40, No. 5, pp. 939–945, 1992
Printed in Great Britain

0956-7151/92 $5.00 + 0.00
Pergamon Press plc

THE WETTING TRANSITION IN HIGH AND LOW ENERGY GRAIN BOUNDARIES IN THE Cu(In) SYSTEM

B. STRAUMAL†, T. MUSCHIK, W. GUST and B. PREDEL

Max-Planck-Institut für Metallforschung and Institut für Metallkunde der Universität, Seestaße 75, D-7000 Stuttgart 1, Fed. Rep. Germany

(Received 11 June 1991; in revised form 1 November 1991)

Abstract—Wetting of two symmetrical tilt grain boundaries, 77° ⟨110⟩ and 141° ⟨110⟩, in synthetic copper bicrystals with a Cu(In) melt was studied in the temperature range 690–990°C. The contact angle at the site of GB intersection with the solid–melt interface was measured. A wetting transition occurred at $T_w = 960 \pm 6$°C for the 77° ⟨110⟩ grain boundary and at $T_w = 930 \pm 5$°C for the 141° ⟨110⟩ grain boundary. The contact angle approached zero for this transition. The relative surface energies of the two boundaries were measured using the thermal grooving technique. The energy of the 77° ⟨110⟩ grain boundary is about 40% lower than that of the 141° ⟨110⟩ grain boundary. Therefore, it has been shown experimentally that the lower the grain boundary energy, the higher the wetting transition temperature. This is in agreement with the thermodynamic model of wetting transitions on grain boundaries.

Résumé—On a étudié la humectation des deux joints des grains symmetriques de flexion 77° ⟨110⟩ et 141° ⟨110⟩ dans les bicrystaux de cuivre syntetiques par l'alliage liquide Cu(In) à l'intervalle des températures de 690 à 990°C. On a mesuré l'angle de contact dans le point de contact de joint des grains avec le joint des phases "solide-liquide". A $T_w = 960 \pm 6$°C pour le joint des grains 77° ⟨110⟩ et à $T_w = 930 \pm 5$°C pour 141° ⟨110⟩ la transition de phase de la humectation a lieu. En moment de cette transition l'angle de contact devient égal à zero. Avec la methode du sillon d'attaque thermique la energie supeficielle relative σ_{GB} des deux joints des grains est mesuré. La σ_{GB} de joint des grains 77° ⟨110⟩ est 0.6 fois plus petit, que la σ_{GB} de joint des grains 141° ⟨110⟩. Donc il est directement demonstré, que transition de phases de la humectation à joints des grains avec la energie superficielle plus petit passe à temperature plus grand, qu'au joints des grains avec la energie superficielle plus grand. Ces factes sont en accord avec la modelle thermodinamique des transitions des phases de la humectation à les joints des grains.

Zusammenfassung—Es wurde die Benetzung zweier symmetrischer Kippkorngrenzen (77° ⟨110⟩ und 141° ⟨110⟩) in diffusionsverschweißten Kupfer-Zweikristallen mit einer Cu(In)-Schmelze im Temperaturbereich zwischen 690 bis 990°C untersucht. Dabei wurde der Kontaktwinkel im Bereich der Schnittlinie der Korngrenze mit der Fest-flüssig-Grenzfläche gemessen. Der Korngrenzenphasenübergang der Benetzung erfolgt für die 77° ⟨110⟩-Korngrenze bei der Benetzungstemperatur $T_W = 960 \pm 6$°C und für die 141° ⟨110⟩-Korngrenze bei $T_W = 930 \pm 5$°C. Der Kontaktwinkel verschwindet bei der Benetzungsübergangstemperatur. Mit der Methode des thermischen Ätzens wurden die relativen Grenzflächenenergien beider Korngrenzen gemessen. Die Korngrenzenenergie der 77° ⟨110⟩-Grenze ist etwa 40% niedriger als die Energie der 141° ⟨110⟩-Korngrenze. Es wurde somit unmittelbar gezeigt, daß der Benetzungsübergang an Korngrenzen mit niedrigeren Grenzflächenenergien bei höheren Temperaturen erfolgt als an Korngrenzen mit höheren Energien. Dies stimmt mit dem thermodynamischen Modell des Benetzungsphasenüberganges an Korngrenzen überein.

1. INTRODUCTION

In recent years two-dimensional phase transformations at interfaces, and wetting transitions in particular, have attracted increasing attention [1–3]. What is a wetting transition? Consider a binary system in which a solid phase α is in contact with a melt L [Fig. 1(a) and (b)]. The angle θ is the angle between the solid–liquid interfaces at the intersection line between the grain boundary (GB) in the solid phase α and the melt L. There exists a temperature T_w above which θ is zero [Fig. 1(b)]. At temperatures far below the wetting transition temperature T_w the angle θ is larger than zero and is slightly dependent on the temperature. θ approaches zero in a small temperature interval near T_w. Such a phenomenon is called a wetting transition.

The thermodynamic explanation of the wetting transition is schematically illustrated in Fig. 1(c), in which the temperature dependencies of the surface energy of a grain boundary, σ_{GB}, and that of a solid–liquid interface, σ_{SL}, are shown. If the surface energy σ_{SL} decreases faster than the GB energy σ_{GB} in a certain temperature range, then the wetting condition

$$2\sigma_{SL} < \sigma_{GB} \qquad (1)$$

will be obeyed above T_w. In this case the formation of a layer of liquid phase on a GB becomes energet-

†Permanent address: Institute of Solid State Physics, Russian Academy of Sciences, Chernogolovka, Moscow District, 142432, Russia.

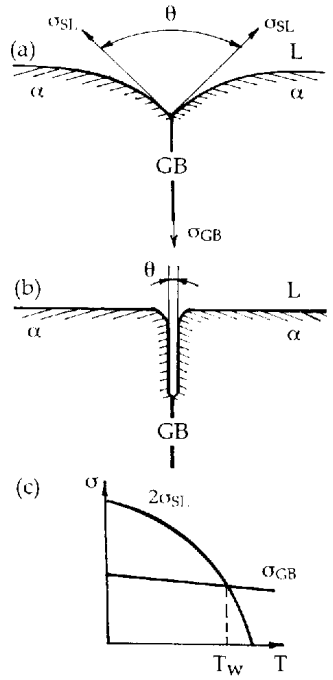

Fig. 1. The shape of the interphase boundary between the solid phase α and the melt L near the contact line with the grain boundary. (a) At $T < T_W$ (T_W is the wetting transition temperature for the grain boundary) the contact angle $\theta > 0$. (b) At $T > T_W$ the contact angle $\theta = 0$. (c) Schematic diagram of the temperature dependencies of the energies of the grain boundaries (σ_{GB}) and the solid–liquid phase boundaries (σ_{SL}) near T_W.

ically favorable. Thus, the contact angle θ becomes zero [Fig. 1(b)], and a wetting transition occurs at $T = T_w$ where $2\sigma_{SL} = \sigma_{GB}$.

The thermodynamic conditions which must be fulfilled for a wetting transition to occur have been considered in detail by Cahn [4], who demonstrated that such a transition must always be observed near a critical point. Let us consider the phase diagram presented in Fig. 2 within the framework of Cahn's ideas. For an alloy of composition C_B in the $\alpha + \beta$ phase field there can exist α/α and β/β grain boundaries as well as α/β interphase boundaries (IBs). Above the critical temperature T_c no α/β IBs are thermodynamically stable in an alloy of this composition, but GBs still do exist. This means that when a critical point is approached from the two-phase region the surface energy of an IB rapidly decreases to zero in a certain temperature range. As was shown in [4], the surface energy $\sigma_{\alpha\beta}$ of IBs decreases faster than $(\sigma_{\alpha\alpha} - \sigma_{\beta\beta})$ as $T \to T_c$. This means that there exists a temperature T_w above which a layer of β phase exists on α/α grain boundaries in the two-phase $\alpha + \beta$ region. In other words, α/α GBs become thermodynamically unstable in the temperature interval between T_w and T_c. (In our simplified model the surface energy of α/α GBs is assumed to be larger than that of β/β GBs at a given temperature, because the melting temperature of component A is higher than that of component B.)

The phase diagram of the Cu–In system studied here differs significantly from the model system treated by Cahn. Critical points, near which the surface energy of IBs decreases rapidly, need not only be stable [Fig. 2(a)], but can also be metastable [Fig. 2(b)]. In the Cu–In system there is no stable critical point. However, we suppose that not only the surface energies of interfaces between two solid phases can decrease near a stable critical point, but also that those of solid–liquid interfaces can decrease near a metastable critical point. Phase transitions associated with the wetting of GBs by a melt have been observed in the following binary systems: Zn–Sn [5, 6], Al–Sn [7–9], Al–Pb [7], Ag–Pb [10], (Fe–Si) Sn [11], (Fe–Si)–Zn [11, 12] and Cu–Bi [13].

It is known that the surface energies of IBs and GBs with different crystallographic parameters can differ significantly. This means that the curves $\sigma_{SL}(T)$ and $\sigma_{GB}(T)$ can intersect at different temperatures, and thus T_w values will differ for different interfaces (Fig. 3). Till now the differences in wetting transition temperatures for different interfaces have not been studied explicitly, because most investigations dealt with polycrystals [5–10], whereas the data of [11–13] were obtained from GBs with one single misorientation value. There is, however, evidence that T_w is different for different GBs. In a study of the melting of polycrystalline Cu–In solid solutions [14] it was shown that the wetting of GBs and the subsequent migration of liquid films at the GBs plays an important role during the melting process. In particular, in alloys quenched from temperatures a few degrees above the melting temperature small droplets of a

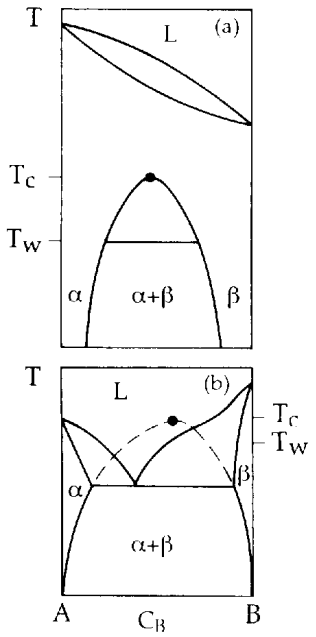

Fig. 2. Hypothetical phase diagrams of systems in which a wetting transition can occur at T_W. (a) A diagram with miscibility gap and a stable critical point. (b) An eutectic diagram with a metastable critical point.

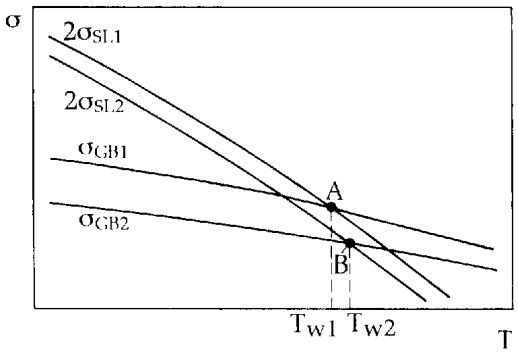

Fig. 3. Schematic diagram of the temperature dependencies of $\sigma_{GB}(T)$ and $\sigma_{SL}(T)$ for grain and interphase boundaries with different interfacial energies. The intersection points A and B correspond to the wetting temperatures of the grain boundaries 1 and 2.

liquid phase were observed at the ends of twin plates, while the coherent twin boundaries of the same twin plate were not wet (Fig. 4). This indicates that the wetting transition on different grain boundaries can occur at different temperatures, if at all. The aim of the present work is to investigate the relationship between the wetting transition of copper GBs wet with a Cu(In) melt and the energy of the GBs. The experiments were performed on diffusion-bonded Cu bicrystals containing symmetric ⟨110⟩ tilt boundaries with various misorientation angles.

2. EXPERIMENTAL

2.1. Selection of the misorientation parameters and production of the bicrystals

In their study of the boundary misorientation dependence of diffusion induced grain boundary migration during the diffusion of zinc into copper Giakupian *et al.* [15] used diffusion-bonded copper bicrystals to evaluate the grain-boundary migration rate v and the diffusion permeability $s\delta D_b$ (here, s is the adsorption factor, D_b the grain boundary diffusion coefficient, and δ the thickness of the GB) of symmetrical ⟨110⟩ tilt GBs with misorientation angles ϕ between 10.1° and 171.9° measured between {110} planes. No zinc penetration and no GB migration was observed for the coherent Σ3 twin GB with misorientation angle $\phi = 70.5°$ about the ⟨110⟩ tilt axis. The minimum measurable values of v and $s\delta D_b$ were observed for the GB with $\phi = 77°$, which is near the coherent twin misorientation. The maximum values of v and $s\delta D_b$ were measured for the GB with $\phi = 141°$ which is close to the Σ9 GB at $\phi = 141.1°$. For the present study the two GBs with the maximum measurable difference in v and $s\delta D_b$ ($\phi = 77°$ and $\phi = 141°$) were chosen.

Cylindrical single crystals (10 mm diameter) of high purity Cu (99.9998 wt%) were grown by the Bridgman technique in high purity graphite crucibles and oriented by Laue X-ray back reflection. Two reference planes on opposite sides of the single crystals parallel to the crystal axis were cut by spark erosion. Then 3 mm slices were cut from the single crystals so that the parallel flat faces of the slices were perpendicular to the crystallographic direction chosen for the GB normal (GBN). After surface preparation of the respective GB planes with a precision mill the slices were put together with the reference planes parallel, and the desired misorientation was obtained by a 180° rotation of one slice with respect to the other around the GBN. The slices were then diffusion-bonded in high vacuum ($<4 \cdot 10^{-4}$ Pa) for 15 h at 1050°C. After bonding, the misorientation was determined by computerized evaluation of back reflection patterns. Samples, approximately $4.5 \times 3 \times 2.5$ mm in size, with the 4.5×3 mm faces parallel to {110} were then cut from the bicrystals. The {110} faces with the 3 mm long GB intersecting the surface at right angles along the center line were finally polished on 4000 grit SiC paper. After cleaning, the samples were annealed for 15 h at 950°C in vacuum ($<4 \cdot 10^{-5}$ Pa) in order to relieve any residual strains. The {110} faces of the specimen for the GB energy measurements were then precision milled to a mirror-like finish and annealed for 60 h at 1040°C in vacuum ($<4 \cdot 10^{-4}$ Pa).

2.2. Wetting experiments

For the wetting experiments an indium layer about 1 mm thick was applied on the two opposite {110} faces of the samples by immersion of the samples in an In melt. The In layer thickness was selected so that the average sample composition after annealing was in the two-phase (Cu)+L phase field [point D in Fig. 5(a)]. After the In deposition, the samples were placed in evacuated quartz ampules with a residual pressure of approx. $4 \cdot 10^{-4}$ Pa. The samples were then annealed for 20 min at various temperatures between 690 and 990°C and subsequently quenched in water. The annealing temperature was maintained constant with an accuracy of ±0.5°C. After quenching, the samples were embedded in a holder using Wood's

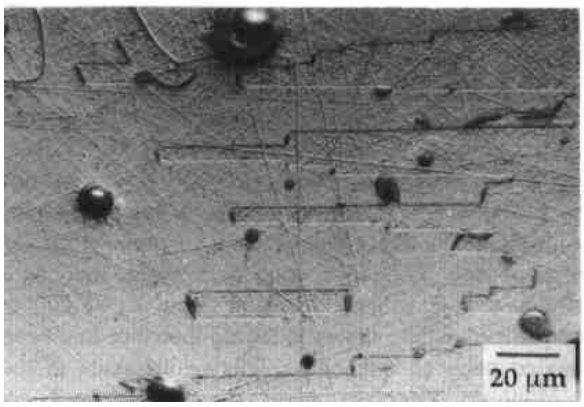

Fig. 4. Light micrograph of a Cu–8.3 at.%. In alloy quenched after heating to a temperature about 10°C above its liquidus temperature with a heating rate of 5°C/min. The coherent twin boundaries (straight boundaries) do not show any indication of a liquid phase, whereas a liquid phase has already formed at the incoherent segments of the GBs.

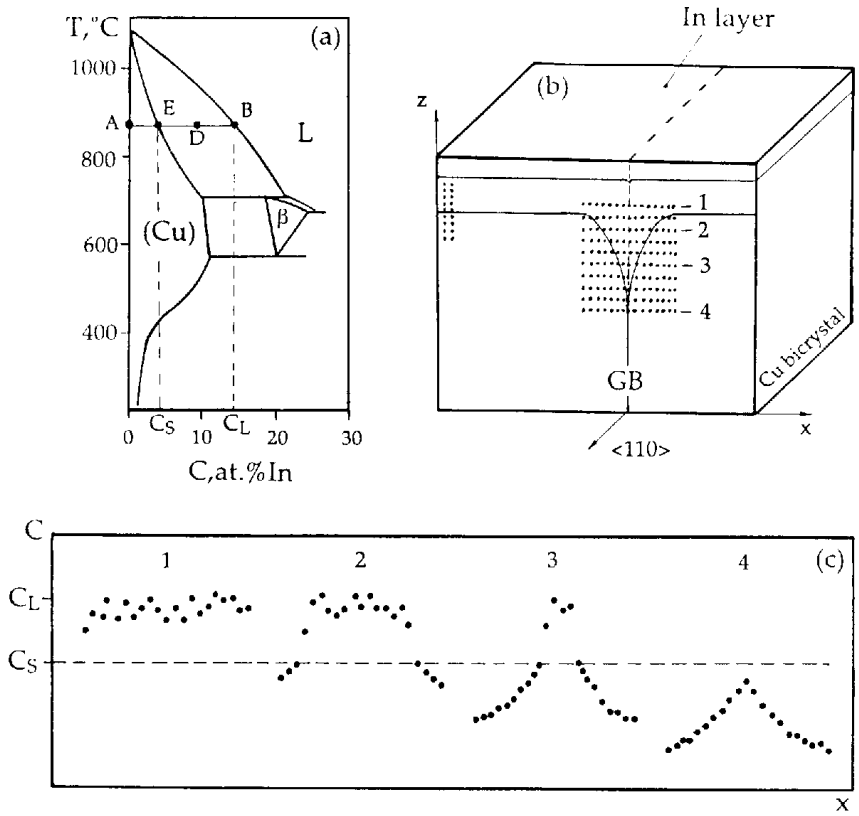

Fig. 5. The determination of the position of the solid–liquid interface with the aid of electron microprobe analysis. (a) Cu–In phase diagram [16, 17] showing the concentrations C of indium in the Cu bicrystal (point A), in the melt near the interface C_L (point B), in the solid near the interface C_S (point E), and the average concentration of In in the sample (point D). (b) The location of the In concentration measurements in the Cu bicrystal after the annealing. (c) Schematic indium concentration profiles. The numbers 1–4 in Fig. 3(b) show the positions of these profiles.

metal and then mechanically ground and polished. The cross-section plane was perpendicular to the GB and the sample surface onto which In had been deposited [see Fig. 5(b)].

In order to observe a GB wetting transition, the angle θ at the contact line of the GB with the liquid phase [Fig. 1(a) and (b)] has to be measured. To do this, it was necessary to determine the position of the solid–liquid interface at the annealing temperature prior to quenching. This was achieved in the present study by determining the indium concentration distribution in the contact region. During annealing, a region of bulk diffusion develops in the solid near the solid–liquid interface. In this region the indium concentration changes from zero [point A in Fig. 5(a)] to the solidus concentration C_S (point E on the solidus line). The liquidus composition C_L of the melt at the solid–liquid interface corresponds to point B on the liquidus line. Therefore, after quenching, there is a sudden change in concentration (from C_S to C_L) at the position where the solid–liquid interface had been located prior to quenching. The coordinates of the solid–liquid interface were thus determined by measuring the indium concentration distribution in the contact region with an electron microprobe.

Concentration profiles were measured by step scanning the electron beam across the boundary with a step length of 1 μm [see Fig. 5(b)]. The step widths between the profiles away from the former specimen surface depended on the penetration depth of the liquid phase into the GB. Their values ranged between 1 and 5 μm. The accuracy of the sample positioning in the JEOL-6400 electron probe microanalyzer used in our studies was ± 1 μm. Figure 5(c) schematically presents selected concentration profiles obtained with this technique. Profile 1 exclusively belongs to the region where the liquid phase had been during annealing, the concentration at all points of the profile being higher than C_S. On profile 2 one can see a smooth decrease of concentration in the zone of bulk diffusion. In the middle of this profile there is a region where $C > C_S$. The sudden change of concentration to C_S is marked by a dashed line. On profile 3 the width of the region with $C > C_S$ is decreased in comparison to profile 2. On profile 4, the sudden change of concentration is no longer present, and the smooth curves of bulk diffusion are connected.

2.3. *Thermal grooving experiments*

Our technique for measuring the GB energy via thermal grooving experiments [18] is described in detail in [19]. Briefly, the thermal groove results from a local equilibrium between GB and surface energies as shown schematically in Fig. 6(a). Neglecting Herring's torque terms [20] and knowing that

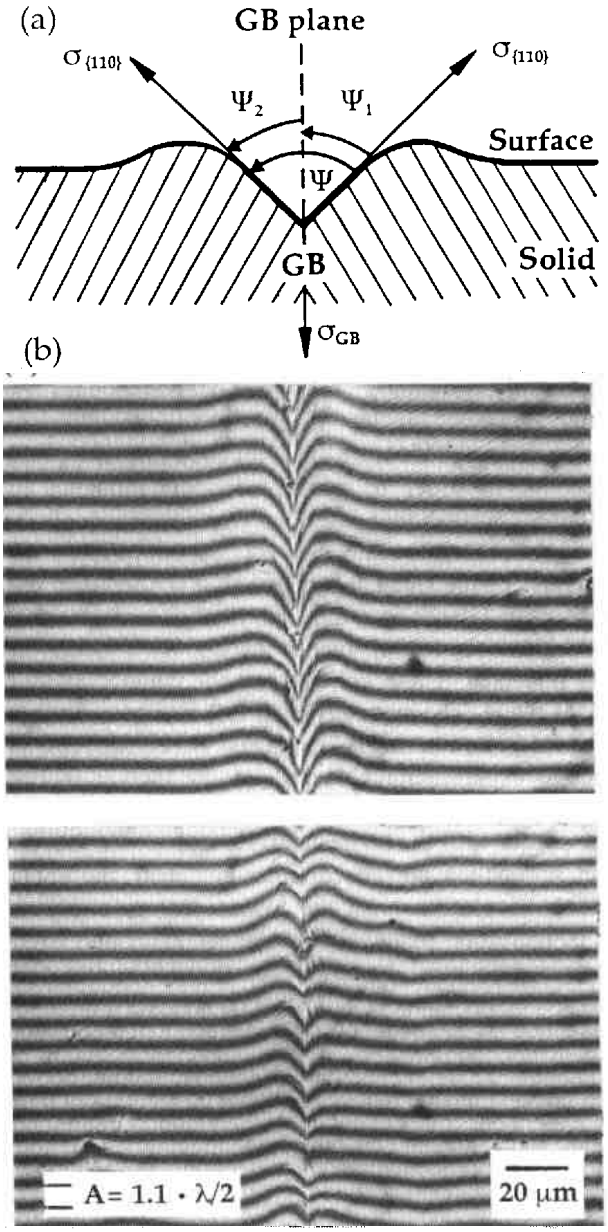

Fig. 6. (a) Schematic diagram of a thermal groove. The dihedral angle Ψ is a measure of the ratio $\sigma_{GB}/\sigma_{\{110\}}$ between the GB energy and the energy of the {110} surface. (b) Typical interference micrographs of the 141° ⟨110⟩ GB (top) and the 77° ⟨110⟩ GB (bottom).

both surfaces are identical (parallel to {110} planes) the equilibrium condition at the intersection line of the interfaces is expressed by

$$\sigma_{GB} = \sigma_{\{110\}} \cos \Psi_1 + \sigma_{\{110\}} \cos \Psi_2 \qquad (2)$$

where $\sigma_{\{110\}}$ is the surface energy of the {110} surface, and Ψ_1 and Ψ_2 are the angles between the GB plane and the tangents to the surfaces on either side of the GB. The GB grooves profiles turned out to be approximately symmetrical with respect to the GB plane. Thus $\Psi_1 = \Psi_2$ and equation (2) reduces to

$$\sigma_{GB}/\sigma_{\{110\}} = 2 \cos \Psi_1. \qquad (3)$$

Thus, the equilibrium angle $\Psi = 2\Psi_1$ is dependent only on the ratio $\sigma_{GB}/\sigma_{\{110\}}$. The theory of thermal grooving predicts that the profiles in the vicinity of the root of a groove are parabolic and can be described by

$$y = ax - bx^2 + c \qquad (4)$$

where x and y are the coordinates parallel and perpendicular to the surface, respectively, and a, b and c are constants. These constants were calculated by least-square fitting of equation (4) to digitized profiles of the groove walls close to the groove root at $x = 0$. The angle Ψ_1 between the GB plane and the surface tangent at $x = 0$ was then calculated using the equation

$$\Psi_1 = 90° - \tan^{-1} a \qquad (5)$$

where a is the slope of the parabolic profile at $x = 0$.

Subsequent to annealing, the GB groove profiles were determined interferometrically using a Leitz interference microscope with a monochromatic Na vapor light source (wavelength $\lambda = 0.589\,\mu$m). The parallel fringe patterns arising from the two beam interference were photographed at a magnification of 500:1 and printed to a final magnification of 2000:1. The groove profiles were then determined from the prints using a Hewlett Packard Series 200 computer equipped with a digitizing pad. The relative displacement A of a fringe in the plane of the print corresponds to a depth of $1.1 \cdot \lambda/2$ on the specimen surface [21]. The values for the dihedral angle were averaged over 20 profiles at characteristic locations on each GB.

3. RESULTS AND DISCUSSION

In Fig. 6(b) selected parts of interference micrographs for the two GBs are shown. It is apparent to the naked eye that the groove of the 141° ⟨110⟩ GB (top) is deeper and has a smaller dihedral angle than the groove of the 77° ⟨110⟩ GB (bottom). The interferometric measurements show that the mean value of the dihedral angle is $\Psi = 164.6° \pm 1.2°$ for the 77° ⟨110⟩ GB and $\Psi = 154.8° \pm 1.2°$ for the 141° ⟨110⟩ GB. According to equation (3) these angles yield relative GB energies of 0.27 and 0.44, respectively. This means that the GB energy of the 77° ⟨110⟩ GB is about 40% less than that of the 141° ⟨110⟩ GB.

The shapes of solid–liquid interfaces at the intersection of the GB with the sample surface are depicted in Fig. 7 for various temperatures. For both the 77° ⟨110⟩ GB [Fig. 7(a)] and the 141° ⟨110⟩ GB [Fig. 7(b)], it is evident that the contact angle θ decreases to zero with increasing temperature. Figure 8(a) and (b) presents the temperature dependencies of the contact angles θ for both GBs. It can be seen that the contact angle θ decreases from ~180° far below T_w to zero at T_w and remains zero above this point. The wetting transition temperatures for the two GBs differ by 30°C ($T_w = 960 \pm 6$°C for the 77° ⟨110⟩ GB and $T_w = 930 \pm 5$ C for the 141° ⟨110⟩ GB).

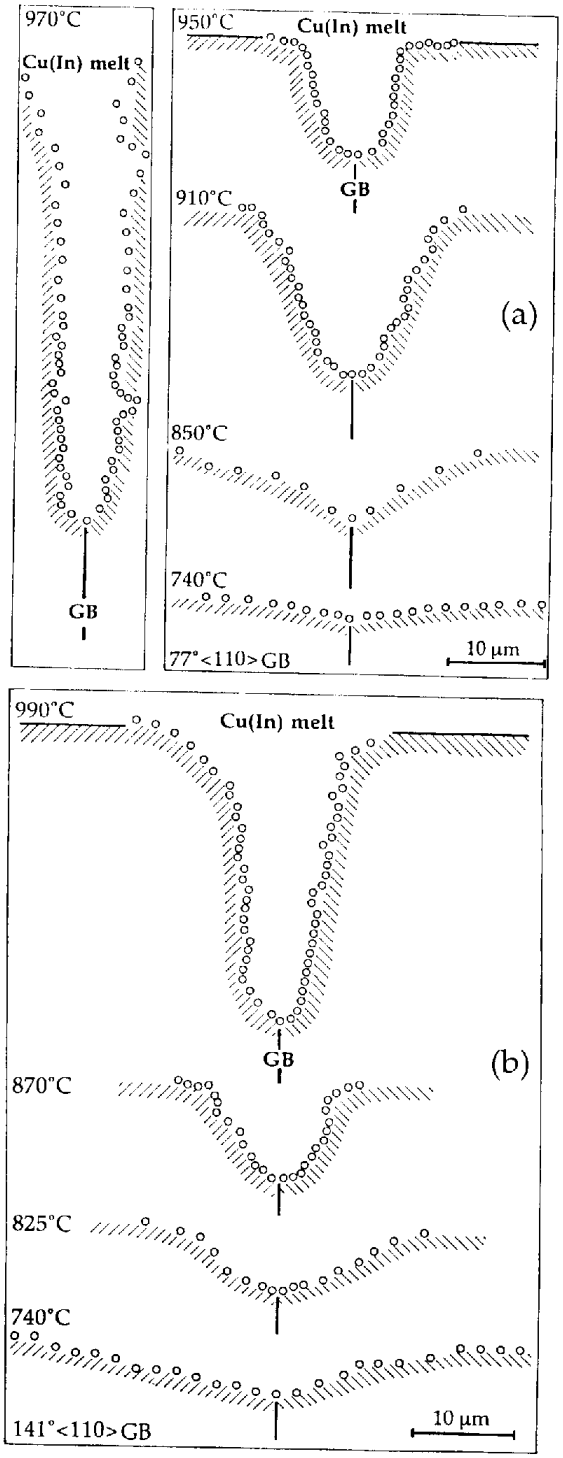

Fig. 7. The shape of solid–liquid interface at the intersection line of a grain boundary with the sample surface for various temperature for the 77° ⟨110⟩ (a) and 141° ⟨110⟩ (b) symmetrical tilt boundaries.

As was mentioned previously the energy of the 77° ⟨110⟩ GB is less than that of the 141° ⟨110⟩ GB. It was also shown in [12] that the migration rate v and the diffusion permeability $s\delta D_b$ of this GB are more than an order of magnitude smaller than the same quantities for the 141°⟨110⟩ GB. This is consistent with the well-known fact that the diffusion permeability and mobility of grain boundaries with low energy are usually lower than the permeability and mobility of grain boundaries with high surface energies [22].

It can be seen from Fig. 8 that the wetting transition temperature of the GB with the lower surface energy is higher than that of the GB with the higher energy. How can this be explained? Referring to Fig. 3 it can be seen that GBs with lower surface energy undergo a wetting transition at a higher temperature if the $2\sigma_{SL}(T)$ curve remains the same. Thus, our results confirm the theoretical prediction that the wetting transition occurs at a higher temperature for grain boundaries with lower surface energy. Different crystallographic planes in contact with the melt, however, can be characterized by the different values of σ_{SL}. This can also affect the value of T_W (see Fig. 3). In order to account for the influence of different solid–liquid interface energies we qualitatively estimate the ratio $\sigma_{SL1}/\sigma_{SL2}$ as the ratio of the energies of the free Cu surfaces that would form the respective GBs. The symmetric tilt GB with $\phi = 77°$ is formed by (988) planes facing each other at the interface. These are close to the densely packed (111) plane. The symmetric tilt GB with $\phi = 141°$ is formed by contacting (411) planes. Theoretical [23] as well as experimental [24] data on the surface energy anisotropy of Cu show that the (411) plane is among the planes with the highest surface energies in Cu. At the same time surface orientations near the (111) plane orientation have the lowest surface energies. It is, therefore, assumed that the σ_{SL} value at a fixed temperature must be lower for the 77° ⟨110⟩ GB than that for the 141° ⟨110⟩ GB. Hence it follows that the $2\sigma_{SL}$ curve for the 77° ⟨110⟩ GB [line $2\sigma_{SL2}(T)$ in Fig. 3] must be placed below the respective curve for the 141° ⟨110⟩ GB [line $2\sigma_{SL1}(T)$ in Fig. 7]. As can be seen from Fig. 3, the temperature of the wetting transition, T_{W2}, for the 77° ⟨110⟩ GB

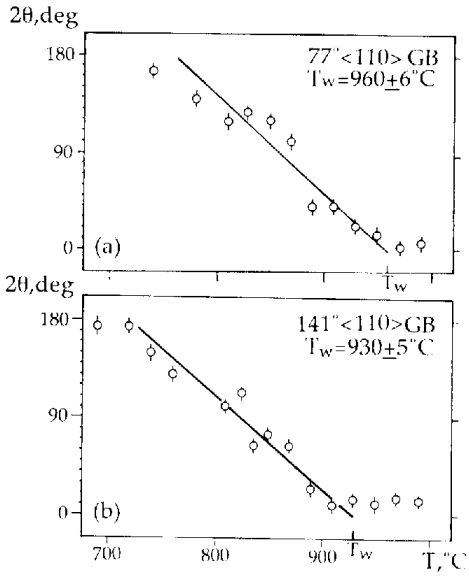

Fig. 8. The temperature dependence of the contact angle θ for the 77° ⟨110⟩ (a) and 141° ⟨110⟩ (b) grain boundaries. The T_{W1} and T_{W2} wetting transition temperatures are determined by the graphical extrapolation to $\theta = 0$.

corresponds to the intersection B of the curves $2\sigma_{SL2}(T)$ and $\sigma_{GB2}(T)$. Similarly, T_{W1} for the 141° ⟨110⟩ GB corresponds to the intersection point A of the curves $2\sigma_{SL1}(T)$ and $\sigma_{GB1}(T)$. We see that the decrease of the GB energy from σ_{GB1} to σ_{GB2} and the decrease of the solid–liquid interphase energy from σ_{SL1} to σ_{SL2} effect T_W "in opposite ways". In other words, the change of σ_{SL} in going from the 77° ⟨110⟩ grain boundary to the 141° ⟨110⟩ grain boundary can only decrease the difference between T_{W1} and T_{W2}. Actually, $T_{W2} > T_{W1}$, and $T_{W2} - T_{W1} = 30°C$ (see Fig. 8). All in all the above considerations lead to the conclusion that what we have really shown experimentally is that the wetting temperature T_W is lower for GBs with higher surface energy.

4. CONCLUSIONS

From the results of our experimental study we conclude the following:

1. The specific grain boundary energies, σ_{GB}, of symmetrical 77° ⟨110⟩ and 141° ⟨110⟩ tilt grain boundaries in synthetic copper bicrystals were measured using the thermal grooving technique. The grain boundary energy of the symmetric 77° ⟨110⟩ tilt grain boundary, which is close to the coherent Σ3 twin boundary, is shown to be about 40% less than that of the 141° ⟨110⟩ grain boundary, which is close to a Σ9 coincidence site boundary.

2. The wetting of these two grain boundaries by a Cu(In) melt was also studied. It was shown that both grain boundaries undergo a wetting transition. This means that the contact angle θ at the intersection line of the grain boundary with the solid-liquid interface approaches zero as the temperature increases to the wetting temperature T_W, and remains zero for $T > T_W$.

3. It was shown that T_{W2}, the wetting transition temperature for the 77° ⟨110⟩ grain boundary, is 30°C higher than T_{W1}, the wetting transition temperature of the 141° ⟨110⟩ grain boundary ($T_{W2} = 960 \pm 6°C$, $T_{W1} = 930 \pm 5°C$). Since the energy of the 77° ⟨110⟩ grain boundary is about 40% less than that of the 141° ⟨110⟩ grain boundary this is in agreement with the thermodynamical model of the transition of grain boundary wetting by melt.

Acknowledgements—The authors are grateful to Professor R. A. Fournelle, Professor L. Shvindlerman, Professor Ch. Herzig and Dr E. Rabkin for fruitful discussions of the results, and to Dr E. Bischoff and Miss A. Holme for their help in operating the electron probe microanalyzer. We also thank Drs B. Giakupian and R. Schmelzle for providing the bicrystalline specimens for this study. One of the authors (B.S.) wishes to thank the Alexander von Humboldt Foundation for the support of his work in Stuttgart.

REFERENCES

1. S. Dietrich, in *Phase Transitions and Critical Phenomena* (edited by C. Domb and J. Lebowitz), Vol. 12, p. 1. Academic Press, New York (1988).
2. M. Schick, *Prog. Surf. Sci.* **11,** 245 (1981).
3. P. G. De Gennes, *Rev. Mod. Phys.* **57,** 827 (1985).
4. J. W. Cahn, *J. chem. Phys.* **66,** 3667 (1977).
5. A. Passerone, N. Eustatopoulos and P. Desre, *J. less-common Metals* **52,** 37 (1977).
6. A. Passerone and R. Sangiorgi, *Acta metall.* **33,** 771 (1985).
7. K. K. Ikeuye and C. S. Smith, *Trans. Am. Inst. Min. Engrs* **185,** 762 (1949).
8. N. Eustatopoulos, L. Coudurier, J. C. Joud and P. Desre, *J. Cryst. Growth* **33,** 105 (1976).
9. J. H. Rogerson and J. C. Borland, *Trans. Am. Inst. Min. Engrs* **227,** 2 (1963).
10. A. Passerone, R. Sangiorgi and N. Eustatopoulos, *Scripta metall.* **16,** 547 (1982).
11. E. I. Rabkin, V. N. Semenov, L. S. Shvindlerman and B. B. Straumal, *Acta metall. mater.* **39,** 627 (1991).
12. L. S. Shvindlerman, W. Łojkowski, E. I. Rabkin and B. B. Straumal, *Coll. Physique C1* **51,** 629 (1990).
13. H. J. Vogel and L. Ratke, *Acta metall. mater.* **39,** 641 (1991).
14. T. Muschik, W. A. Kaysser and T. Hehenkamp, *Acta metall.* **37,** 603 (1989).
15. B. Giakupian, R. Schmelzle, W. Gust and R. A. Fournelle, *Coll. Physique C1* **51,** 489 (1990).
16. T. Muschik and T. Hehenkamp, *Z. Metallk.* **78,** 358 (1987).
17. T. B. Massalski *et al.* (editors), *Binary Alloy Phase Diagrams*, p. 926. Am. Soc. Metals, Metals Park, Ohio (1986).
18. W. W. Mullins, *J. appl. Phys.* **28,** 333 (1957).
19. R. Schmelzle, T. Muschik, W. Gust and B. Predel, *Scripta metall. mater.* **25,** 1981 (1991).
20. C. Herring, in *The Physics of Powder Metallurgy* (edited by W. E. Kingston), p. 143. McGraw-Hill, New York (1951).
21. F. R. Tolmon and J. G. Wood, *J. Sci. Instr.* **33,** 236 (1956).
22. I. Kaur and W. Gust, *Fundamentals of Grain and Interphase Boundary Diffusion*, p. 287. Ziegler Press, Stuttgart (1989).
23. U. Wolf, P. Gumbsch, H. Ichinose and H. F. Fischmeister, *Coll. Physique C1* **51,** 539 (1990).
24. M. McLean and B. Gale, *Phil. Mag.* **20,** 1033 (1969).